ACS APPLIED NANO MATERIALS

www.acsanm.org

Article

# Radial Junctions on Laser-Cutting Tinplate Enable Semitransparent Thin-Film BIPVs with Low Reflection and Designable Transmission

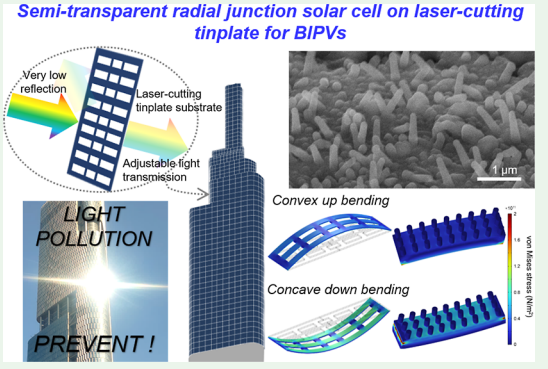
Shaobo Zhang,* Shuyi Wang, Ruijin Hu, Yunqing Cao, Zongguang Liu, Junzhuan Wang, and Linwei Yu*

Cite This: *ACS Appl. Nano Mater.* 2024, 7, 20536−20543

Read Online

ACCESS | Metrics & More | Article Recommendations | Supporting Information

**ABSTRACT:** Semitransparent thin-film solar cells, especially those fabricated directly on building materials, have attracted much interest in the continuously increasing demands of building-integrated photovoltaic (BIPV) applications. Herein, radial junction (RJ)-structured hydrogenated amorphous silicon (a-Si:H) thin-film solar cells, directly constructed upon silicon nanowires (SiNWs) grown by a vapor−liquid−solid (VLS) process on the rough surface of the tinplate substrates, have been successfully demonstrated. After optimizing the SiNW density, an efficiency of 5.89% can be achieved, with an average value of 5.38 ± 0.39%. Compared to the conventional thin-film photovoltaics on glass substrates, the semitransparent RJ-structured thin-film solar cells on the laser-cutting tinplate substrates have a lower reflectivity, an adjustable/designable light transmission, as well as excellent mechanical stability. More importantly, tinplate and other steel/metal substrates can be used as construction materials; thus, the overall costs, including fabrication and installation costs as well as the building construction cost, can be largely reduced. These results highlight the promising potential of the RJ thin film technology on laser-cutting steel/metal substrates to fabricate low-cost, low-reflection, and mechanically stable semitransparent thin-film BIPV devices.



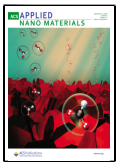

**KEYWORDS:** *radial junction, VLS, BIPV, thin film solar cell, semitransparent*

## 1. INTRODUCTION

Recently, semitransparent photovoltaics have attracted much interest for their light transmission properties, as well as their light weight and durability,[1−4] to meet the continuously increasing demands of building-integrated photovoltaic (BIPV) applications.[5−7] However, light pollution caused by reflected light from conventional glass curtain walls among the skyscraper buildings, as shown in Figure 1b, is an urgent and important issue that should be addressed.[8−10] More importantly, a further cut-down of cost is an important issue too, including fabrication cost, installation cost, and building construction cost.[11,12] Thus, directly fabricating thin-film solar cells upon building materials to reduce the cost, such as tinplate, stainless steel, and other steel/metal substrates, may be a promising method to boost the development of BIPVs.[13,14] In comparison with the semitransparent solar cells based on organic, cadmium telluride (CdTe), copper indium gallium selenium, and perovskite materials,[15−21] hydrogenated amorphous silicon (a-Si:H) thin film technology may be a better choice to fabricate high-performance and robust semitransparent BIPVs, for its nontoxicity, abundant reserves, low cost, industry-mature fabrication technology, and so on.[22−26]

However, the directly deposited planar thin films on the unstable surface of the flexible/bendable substrates are highly vulnerable to the influence of mechanical bending, leaving large/long cracks and even peeling off segments, especially when the used Si-based thin-film light absorption layer has a large thickness >1 $\mu$m even larger. Furthermore, the market-available thin tinplate and other steel/metal substrates usually have a relatively rough surface,[27,28] as shown in Figure 1d,e, which will result in a worse quality of directly deposited thin films. The 3D vertically standing nanostructures can host/support the subsequently deposited a-Si:H thin film, making the main working region out-of-plane and far away from the stress-rich surface, thus achieving excellent mechanical stability.[29,30] Besides, among such 3D frameworks, a strong light trapping effect can be realized, thus resulting in a largely reduced light reflection and allowing a very thin light absorber.[31,32] The RJ, which is made up of the radially stacked p−i−n multilayers deposited around silicon nanowires (SiNWs) directly grown on the surface of the flexible substrate via a vapor−liquid−solid (VLS) process, should be a better and easier choice.[32,33] Compared to the complex and expensive preparation process of "top-down" nanostructures, the

**Received:** June 20, 2024
**Revised:** August 22, 2024
**Accepted:** August 23, 2024
**Published:** September 3, 2024



Downloaded from pubs.acs.org/aanmf6/article-pdf/7/17/20536/3190604/an4c03527.pdf by NANJING UNIV user on 04 November 2026


© 2024 American Chemical Society

https://doi.org/10.1021/acsanm.4c03527
*ACS Appl. Nano Mater.* 2024, 7, 20536−20543

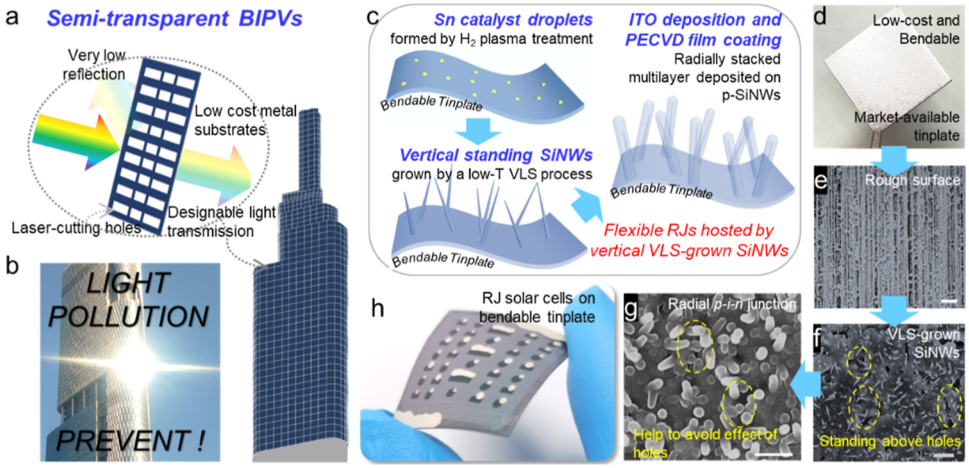



**Figure 1.** (a) Schematic diagram of semitransparent radial junction (RJ) thin-film BIPV devices. (b) Photograph of light pollution caused by the glass curtain wall of the building. (c) Illustrations of the fabrication procedure on the tinplate substrates. (d) Photograph of the tinplate substrate with a size of 2.5 cm × 2.5 cm. (e) Microscopic images of the tinplate substrate. Scanning electron microscopy (SEM) images of (f) VLS-grown SiNWs and the (g) radial p−i−n junction. (h) Photograph of bendable RJ solar cells. The scale bar in (e) is 100 $\mu$m and the others are 1 $\mu$m.

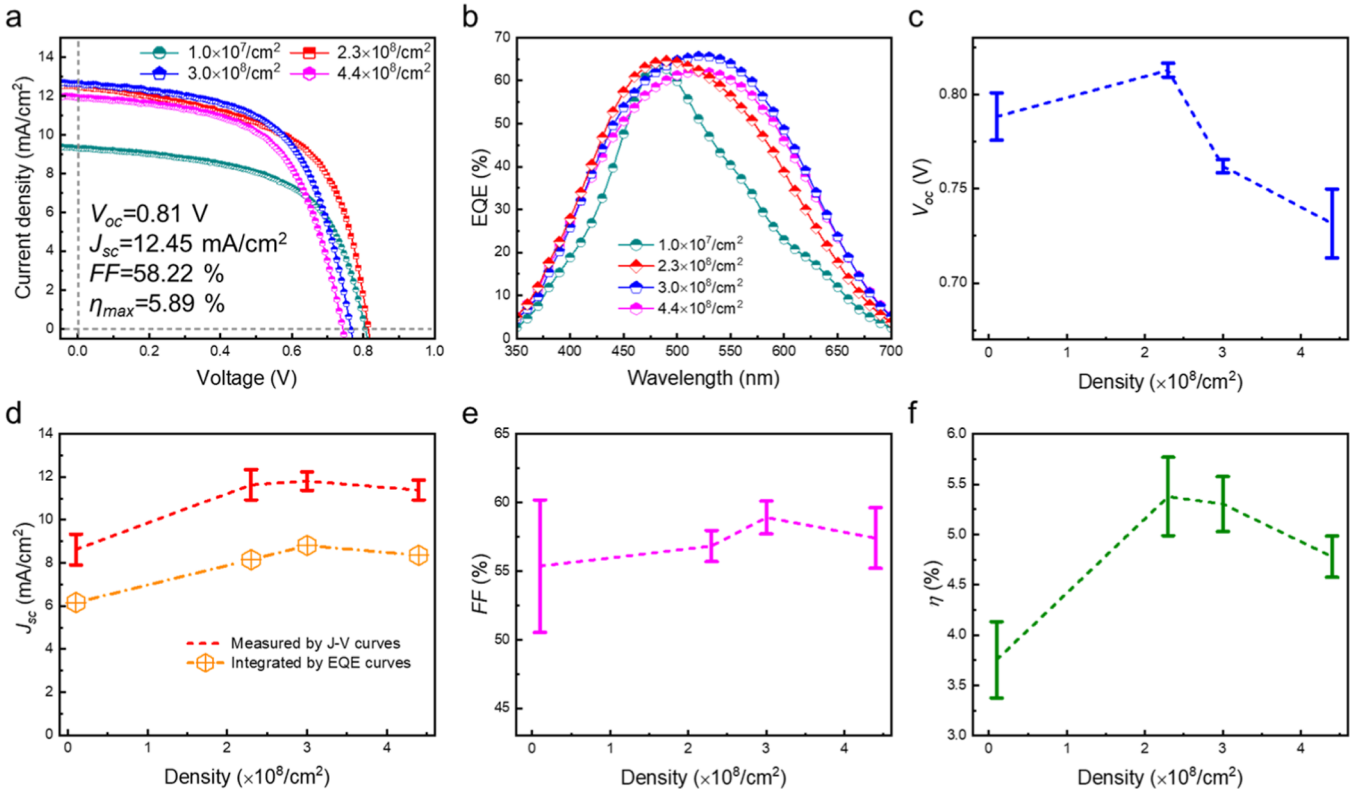



**Figure 2.** (a) Measured $J-V$ curves, (b) EQE curves, and (c−f) average value along with the standard deviation of $V_{oc}$, $J_{sc}$, FF, and $\eta$ of the RJ units on tinplate substrates with varying densities ranging from 1.0 × $10^7$/cm$^2$ to 4.4 × $10^8$/cm$^2$ as well as integrated $J_{sc}$ from EQE curves in (d).

"bottom-up" VLS growth of SiNWs is mediated by the low-melting-point metal catalysts, such as tin (Sn), indium (In), gallium (Ga), and their alloy, thus allowing a rather low fabrication temperature down to 350 °C in the plasma-enhanced chemical vapor deposition (PECVD) system[34,35] and showing good compatibility with the industrial roll-to-roll technology.[36] Thus, the RJ thin film technology directly fabricated on steel/metal substrates has a promising potential to boost high-performance and robust thin film BIPV devices, especially for large-area/scale fabrication.

In this work, by using a VLS-grown SiNW framework to host the deposited a-Si:H thin film, the RJ units have been directly fabricated on the rough surface of the tinplate substrate to demonstrate light-transmission-designable semi-transparent Si-based thin film BIPVs, as schematically drawn in Figure 1a. After optimizing SiNW density, a remarkable efficiency of 5.89% has been achieved, with an average value of 5.38 ± 0.39%, when the SiNW density is 2.3 × $10^8$/cm$^2$. The vertically standing 3D SiNW framework can not only result in a rather lower reflection but also an excellent mechanical stability. Therefore, combined with designable/adjustable


https://doi.org/10.1021/acsanm.4c03527
ACS Appl. Nano Mater. 2024, 7, 20536−20543

Downloaded from pubs.acs.org/aanmf6/article-pdf/7/17/20536/3190604/an4c03527.pdf by NANJING UNIV user on 04 November 2026

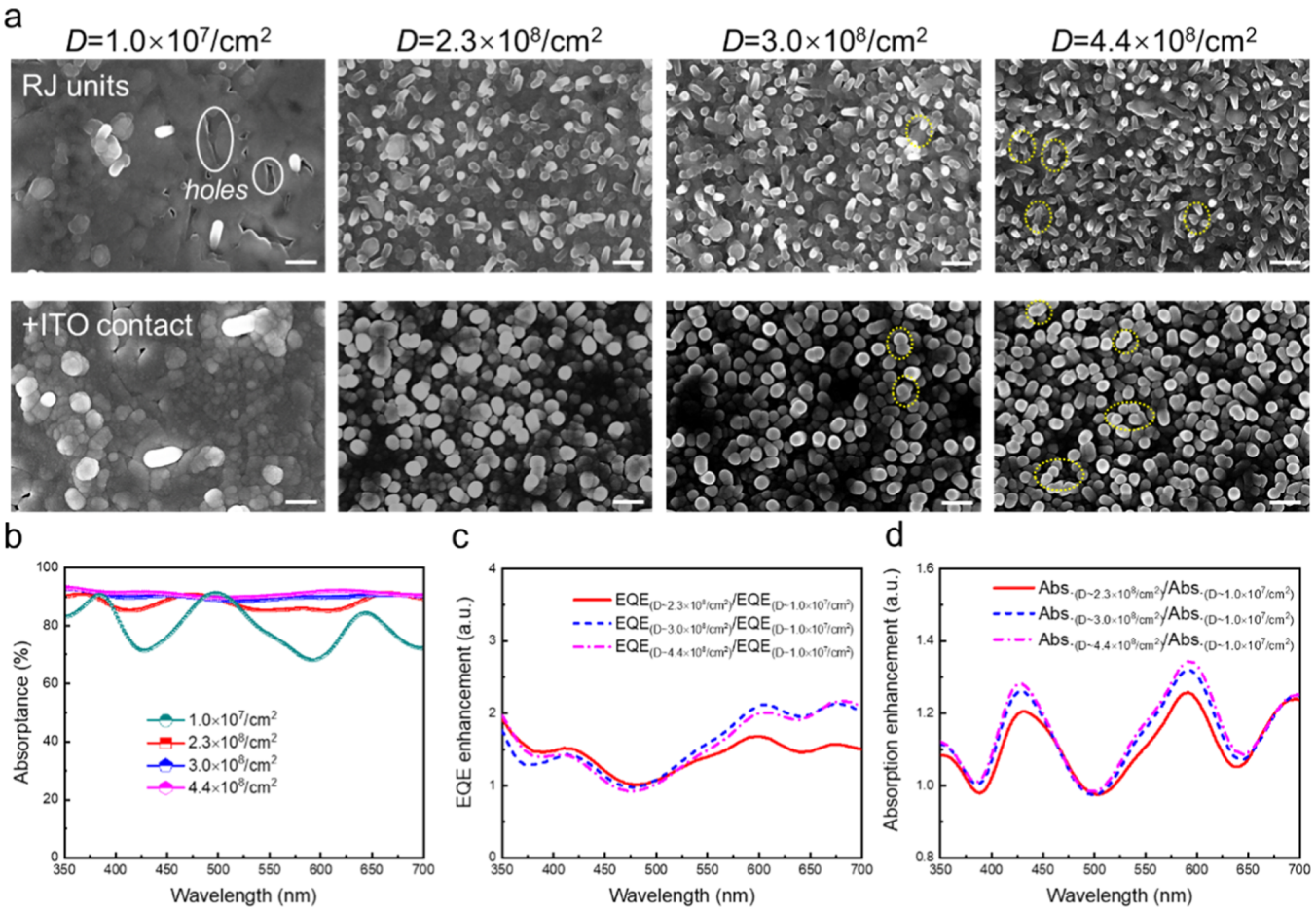



**Figure 3.** (a) SEM images of the RJ units directly built upon the VLS-grown SiNWs with different densities ranging from $1.0 \times 10^7/cm^2$ to $4.4 \times 10^8/cm^2$. SEM images in the upper row show the RJs without the ITO layer, while those with the ITO layer are in the lower row. When at a higher density up to $4.4 \times 10^8/cm^2$, the RJs merge at the top, as indicated by yellow circles. (b) Light absorption curves of the RJ units, as well as (c) EQE enhancement ratio ($EQE_{D\sim2.3\times10^8/cm^2}/EQE_{D\sim1\times10^7/cm^2}$, $EQE_{D\sim3.0\times10^8/cm^2}/EQE_{D\sim1\times10^7/cm^2}$, and $EQE_{D\sim4.4\times10^8/cm^2}/EQE_{D\sim1\times10^7/cm^2}$) and (d) absorption enhancement ratio ($Abs._{D\sim2.3\times10^8/cm^2}/Abs._{D\sim1\times10^7/cm^2}$, $Abs._{D\sim3.0\times10^8/cm^2}/Abs._{D\sim1\times10^7/cm^2}$, and $Abs._{D\sim4.4\times10^8/cm^2}/Abs._{D\sim1\times10^7/cm^2}$). All scale bars are 1 $\mu$m.

laser-cutting metal/steel substrates, the RJ-structured thin film technology could be a promising strategy to fabricate high-performance, low-cost, low-reflected, robust semitransparent BIPV devices.

## 2. EXPERIMENTAL METHODS

**2.1. Device Fabrication.** As schematically shown in Figure 1c, the VLS-grown SiNW-supported RJ thin film solar cells were directly fabricated on the rough surface of 200 $\mu$m thick tinplate substrates (Figure S1), which is made up of p-type SiNWs/intrinsic a-Si:H layer/n-type a-Si:H layer/indium tin oxide (ITO) layer. First, a nominal 4 nm thick Sn catalyst was evaporated onto the tinplate substrate and then loaded into the PECVD system to remove the surface oxide layer and form Sn nanodroplets by hydrogen ($H_2$) plasma. Second, a mixture of $H_2$, silane ($SiH_4$), and diborane ($B_2H_6$) was introduced as the gas source to grow p-SiNWs (Figure 1f). Then, an intrinsic a-Si:H thin film was directly deposited around the SiNWs, by a plasma of $H_2$ and $SiH_4$, followed by the n-type a-Si:H layer, with phosphine ($PH_3$) as the dopant gas, as shown in Figure 1g. Finally, the transparent ITO layer was sputtered on the RJs as the top electrode. The normal section and radially stacked p−i−n multilayer structure of the RJ units have been schematically drawn, as shown in Figure S1f,g. Besides, such radially stacked multilayers have been characterized in our previous work.[29,37]

**2.2. Device Characterizations.** The morphology of RJ units on tinplate substrates was characterized by SEM (Zeiss Sigma). The photocurrent density−voltage ($J-V$) curves were measured under standard AM1.5G illumination conditions (Newport, Oriel Sol-1A). The external quantum efficiency (EQE) curves were measured with a calibrated silicon detector by using the QEX-10 system, and the light absorption was measured by using a UV−vis−NIR spectrophotometer (UV-3600 Plus, Shimadzu).

## 3. RESULTS AND DISCUSSION

Figure 1h shows a photograph of the bendable RJ thin film solar cells fabricated on the tinplate substrates as well as typical top-view SEM images of the VLS-grown SiNW and RJ units in Figure 1f,g, respectively. The firmly standing SiNW on the surface of flexible substrates can host/support the out-of-plane RJ portions, thus allowing them to be well protected and separated from the stress-rich and unstable bottom surface of the mechanically bent substrate. More importantly, a strong light trapping effect actually exists between such vertically standing RJ units, enabling sufficient light harvesting to achieve a large enough photocurrent. Optimizing the density to ensure a uniformly deposited thin film around randomly distributed/oriented SiNWs is an important factor in forming high-quality RJ units for high performance; however, this is a trade-off to

Downloaded from pubs.acs.org/aanmf6/article-pdf/7/17/20536/3190604/an4c03527.pdf by NANJING UNIV user on 04 November 2026


https://doi.org/10.1021/acsanm.4c03527
ACS Appl. Nano Mater. 2024, 7, 20536−20543

Table 1. Comparison of This Work to Other a-Si:H Thin-Film Solar Cells in the Published Literature

| substrate | type | $V_{oc}$ (V) | $J_{sc}$ (mA/cm$^2$) | FF (%) | $\eta$ (%) | refs |
|---|---|---|---|---|---|---|
| stainless steel | radial n−i−p junction $\mu$c-Si:H | 0.48 | 13.42 | 35 | 2.25 | 38 |
| stainless steel | radial n−i−p junction $\mu$c-Si:H | 0.62 | 13.36 | 43 | 3.57 | 39 |
| Al foil | radial p−i−n junction a-Si:H | 0.71 | 14.2 | 56.0 | 5.6 | 30 |
| AZO glass | radial p−i−n junction a-Si:H | 0.73 | 11.8 | 62.0 | 5.3 | 30 |
| PET + ITO + Ag back-reflector | planar p−i−n junction a-Si:H | 0.795 | 7.14 | 58 | 3.30 | 40 |
| PI + ITO + Ag back-reflector | planar p−i−n junction a-Si:H | 0.782 | 7.41 | 58 | 3.36 | 40 |
| photo paper + ITO + Ag back-reflector | planar p−i−n junction a-Si:H | 0.571 | 6.05 | 32 | 1.08 | 40 |
| stainless steel | planar n−i−p junction a-Si:H | 0.93 | 8.90 | 61 | 5.12 | 41 |
| plastic substrate + hybrid polymer + Ag + ITO | planar p−i−n junction a-Si:H | 0.75 | 7.7 | 56.5 | 3.26 | 42 |
| plastic substrate + hybrid polymer + Ag + ITO | hexagonal-pyramid nanostructured planar p−i−n junction a-Si:H | 0.73 | 11.3 | 54.2 | 4.47 | 42 |
| spin coated flat PI + Ag + AZO | planar p−i−n junction a-Si:H | 0.797 | 9.13 | 50.1 | 3.64 | 43 |
| 0.5 aspect-ratio nanocone PI + Ag + AZO | nanocone-structured planar p−i−n junction a-Si:H | 0.820 | 12.95 | 66.5 | 7.06 | 43 |
| 1.0 aspect-ratio nanocone PI + Ag + AZO | nanocone-structured planar p−i−n junction a-Si:H | 0.652 | 11.59 | 34.7 | 2.62 | 43 |
| Kapton polymer + Cr + Al + ITO | planar p−i−n junction a-Si:H | 0.88 | 12.48 | 72 | 7.9 | 44 |
| Kapton polymer + Cr + Al + ITO nanoparticles | planar p−i−n junction a-Si:H | 0.87 | 13.59 | 70 | 8.27 | 44 |
| tinplate | radial p−i−n junction a-Si:H | 0.81 | 12.45 | 58.22 | 5.89 | in this work |

light absorption behavior. Therefore, the $J-V$ characteristics of these RJ solar cells are presented in Figure 2a, as well as the corresponding average values along with the standard deviations of $V_{oc}$, $J_{sc}$, FF, and $\eta$ in Figure 2c−f, respectively, to examine the consequence of the different RJ densities. The RJ density can be calculated by the RJ units without the ITO layer in the corresponding SEM images shown in the upper panel in Figure 3a, ranging from $1 \times 10^7$/cm$^2$ to $4.4 \times 10^8$/cm$^2$, which can also be referred to as the SiNW density, as well as the SEM images for ITO-coated RJ units in the lower panel. Although the numbers vary from batch to batch, usually we have 6−12 effective working cells for being counted at each the same density value. The value of $V_{oc}$ is 0.79 ± 0.012 V for the lowest density of SiNWs ($1.0 \times 10^7$/cm$^2$) that is just catalyzed by the self-provided Sn of the tinplate without using any additionally evaporated catalyst. The self-provided Sn layer of the tinplate is transformed into Sn nanoballs after $H_2$ plasma treatment, as shown in Figure S2a, and the following plasma treatments of amorphous thin film deposition make these Sn nanoballs bigger and easier to observe, as seen in the SEM images in Figure S2b−d. When using an additionally evaporated Sn catalyst layer and a series of proper controls, the $V_{oc}$ reaches a maximum value of 0.81 ± 0.004 V with a SiNW density of $2.3 \times 10^8$/cm$^2$. However, a higher SiNW density ($3.0 \times 10^8$/cm$^2$) results in a rapid drop of $V_{oc}$ to 0.76 ± 0.004 V, and a further increase of SiNW density ($4.4 \times 10^8$/cm$^2$) results in an eventual drop of $V_{oc}$ down to 0.73 ± 0.018 V. The first augment of $V_{oc}$ can be assigned to the support of suitable-density SiNWs, which enables a high-quality deposition of radially stacked thin films than those directly deposited on the rough surface of tinplate substrates, avoiding the negative effect of large numbers of cracks and holes on the tinplate surface, as shown in Figures 3a and S2c.

The measured $J_{sc}$ is found to increase up to 11.64 ± 0.71 mA/cm$^2$ and reach a maximum of 11.81 ± 0.43 mA/cm$^2$ at a SiNW density of $2.3 \times 10^8$/cm$^2$ and $3.0 \times 10^8$/cm$^2$, respectively. However, a further increase of the SiNW density leads to an eventual drop of $J_{sc}$ to 11.39 ± 0.46 mA/cm$^2$ at a higher density of $4.4 \times 10^8$/cm$^2$. To resolve the evolution trend of the photocurrent generation, the EQE curves are measured and presented in Figure 2b, as well as the variation trend of $J_{sc}$ values integrated from EQE curves in Figure 2d, which is consistent with that of extracted $J_{sc}$ in the measured $J-V$ curves. As the SiNW density increases, the first increase in $J_{sc}$ might arise from the improved light absorption, as shown in Figure 3b. With a higher SiNW density at $4.4 \times 10^8$/cm$^2$, the light absorption shows a saturation without any decrease (Figure 3d), while the EQE decreases (Figure 3c), which suggests that the $J_{sc}$ and the EQE of the RJ-structured cells are limited by the carrier collection but not by light absorption. With the increase of the SiNW density, more and more nonuniform coating of RJs can be observed from the SEM images, which can be assigned to the problem of conformal deposition of a-Si:H thin film upon a dense SiNW array. At a low SiNW density, most RJ units are separated from neighboring units, and the coating of the PECVD-deposited a-Si:H thin film seems to be fairly uniform. As shown in Figure S3a,b, enlarged SEM images provide more details that the a-Si:H coating can be deposited with a uniform diameter along the full length of RJ units when the SiNW density is reasonable. However, at a higher SiNW density, more crossing and overlapping between neighboring RJ units can be observed in the SEM images, as marked by the yellow circles shown in the SEM images in Figure 3a. As presented in Figure S3c−e, the RJ cells fabricated on a denser SiNW array would touch each other more easily and even exhibit a twisted geometry. Thus, after optimizing the SiNW density, a remarkable efficiency of 5.89% has been achieved, with an average value of 5.38 ± 0.39%, when the SiNW density is $2.3 \times 10^8$/cm$^2$.

To further highlight the potential of RJs on the tinplate substrate, the $J-V$ curves of RJ solar cells fabricated on the glass and tinplate substrates are plotted in Figure S4a for comparison, as well as the corresponding $V_{oc}$, $J_{sc}$, FF, and $\eta$ are compared and summarized in Figure S4f. With the same RJ density, the solar cells fabricated on the glass substrate have a lower $J_{sc}$ (11.63 mA/cm$^2$) but a larger $V_{oc}$ (0.83 V) and FF (62.56%) compared to those (12.45 mA/cm$^2$, 0.81 V, and 58.22%, respectively) on the tinplate substrate, which is

Downloaded from pubs.acs.org/aanmf6/article-pdf/7/17/20536/3190604/an4c03527.pdf by NANJING UNIV user on 04 November 2026



https://doi.org/10.1021/acsanm.4c03527
ACS Appl. Nano Mater. 2024, 7, 20536−20543

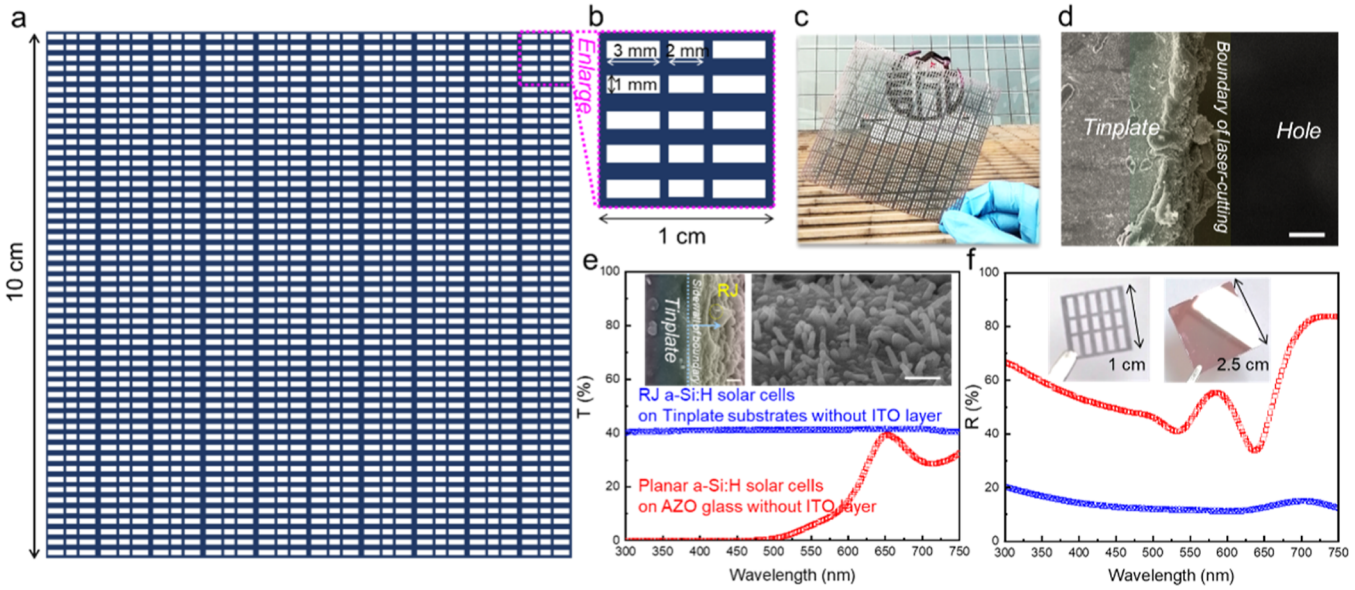



**Figure 4.** (a) Schematic diagram of the design for semitransparent RJ thin-film solar cells (10 cm × 10 cm) and (b) partial enlargement (1 cm × 1 cm), where the white areas are laser-cutting holes to pass through sunlight and other areas are working regions. (c) Photograph of semitransparent RJ solar cells on laser-cutting tinplate substrates. (d) SEM image of the laser-cutting boundary. (e) Transmission spectrum of RJ units on laser-cutting tinplate substrates and planar ones on glass substrates (inset: left is the side-view SEM image of the boundary; right is the side-view SEM image of standing RJ units). (f) Reflection spectrum of RJ solar cells on tinplate substrates and planar ones on glass substrates (inset: left is the photograph of RJ solar cells on laser-cutting tinplate substrates; right is the photograph of planar thin-film solar cells on glass substrates). The scale bar in (d) is 20 $\mu$m and the others are 1 $\mu$m.

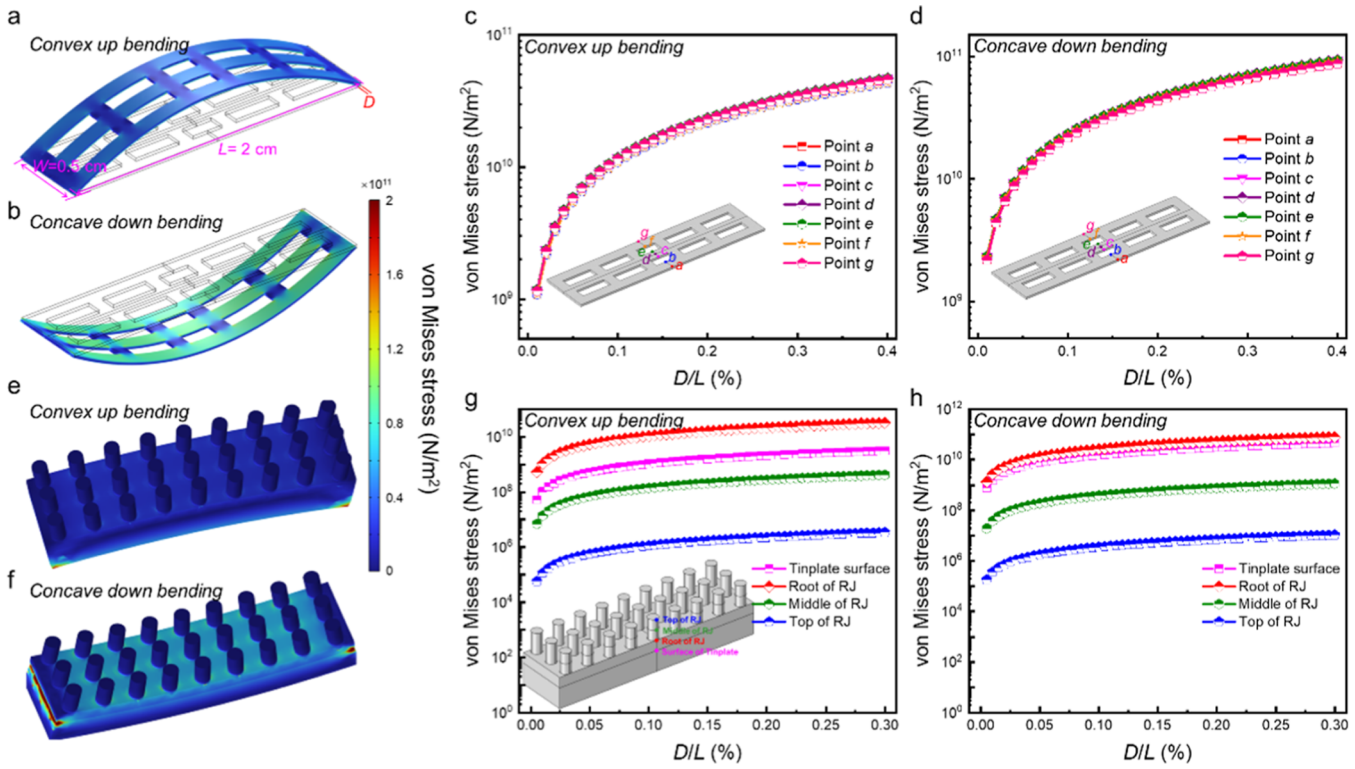



**Figure 5.** Simulated von Mises stress distribution of the laser-cutting tinplate substrate for (a) convex-up and (b) concave-down bending, as well as the extracted stress values as a function of the relative movement $D/L$ for (c) convex-up and (d) concave-down bending. Simulated von Mises stress distribution of the RJ unit on the tinplate substrate for (e) convex-up and (f) concave-down bending conditions, as well as the extracted stress values as a function of the relative movement $D/L$ for (g) convex-up and (h) concave-down bending of bendable tinplate substrates.

consistent with the EQE curves presented in Figure S4b. While switching to a higher SiNW density ($3.6 \times 10^8$/cm$^2$) on the glass substrate, a larger $J_{sc}$ (13.97 mA/cm$^2$) can be achieved but with a lower $V_{oc}$ (from 0.83 to 0.78 V) and FF (from 62.56 to 56.85%). These observations indicate that (1) a reasonable/suitable SiNW density does ensure a good quality of the



https://doi.org/10.1021/acsanm.4c03527
ACS Appl. Nano Mater. 2024, 7, 20536−20543

Downloaded from pubs.acs.org/aanmf6/article-pdf/7/17/20536/3190604/an4c03527.pdf by NANJING UNIV user on 04 November 2026

deposited thin film even on an uneven surface to enable an efficient carrier collection; (2) the Sn nanoballs (as shown in Figure S2) formed by the self-provided Sn layer on the tinplate surface do not show a negative effect on the performance of RJ thin film solar cells; (3) the back-reflection of the tinplate substrate can help to achieve a larger $J_{sc}$ and light absorption, as shown in Figure S4; (4) a denser SiNW array can improve light absorption, but worsen carrier collection, due to a nonuniform coating of the a-Si:H thin film.

Meanwhile, compared to other Si-based thin film solar cells in the published literature,[30,38−44] as summarized in Table 1, the RJ solar cells on tinplate substrates have a remarkable efficiency of 5.89%, especially among these samples fabricated on steel/metal substrates. In addition, the "bottom-up" self-assembling VLS method can avoid the additional nanopattern process to simplify the fabrication process and reduce the fabrication cost, which can help integrate the RJ structures into the industrial mature roll-to-roll technology for large-area fabrication. Besides, tinplate and other steel/metal substrates can be directly used as construction materials, not only saving the installation cost to a large extent but also reducing the construction cost as no additional reinforcement of the building to host the solar cell modules is needed.

Furthermore, the tinplate and other steel/metal substrates can be made semitransparent by using laser-cutting technology, as shown in Figure S5, and can allow a designable/adjustable light transmission by cutting/shaping holes, as shown in Figure 4a. Considering that the line-produced solar cells usually have a size of decimeters and even meters, the tinplate and other steel/metal substrates with millimeter-sized or centimeter-sized holes should be esthetic enough for practical BIPV applications, as seen, for example, in Figure 4c. The light transmission of the laser-cutting tinplate substrate can be easily calculated by using the area of holes divided by the total area. Taking the design in Figure 4b as an example, the fabricated RJ-structured samples on laser-cutting tinplate substrates have a light transmittance of ∼40% in the full wavelength range, as shown in Figure 4e. For comparison, the planar thin-film solar cells deposited on the conventional glass substrates usually have nearly zero light transmission at short wavelength (<500 nm), which is determined by the thickness and quality of the deposited a-Si:H thin film and would affect the real sensory perception to external scenery. More importantly, as shown in Figure 4f, compared to the nearly >50% reflection of conventional planar a-Si:H thin-film solar cells on the glass substrate, the a-Si:H RJ solar cells can have a lower light reflection <20% because of the strong light trapping effect realized among 3D standing RJ arrays.

In addition, it is noteworthy that the direct construction of such 3D RJ units upon the tinplate substrates brings a possible route to fabricate mechanically stable bendable thin film solar cells. The finite element simulation has been carried out, by fixing one edge of the tinplate substrate and moving another edge (as shown in Figure S6), to discover the von Mises stress distribution for convex-up bending and concave-down bending conditions. The simulated stress distributions of laser-cutting substrates are presented in Figure 5a,b for convex-up and concave-down conditions, respectively, as well as the extracted stress values at seven different points as a function of the relative movement $D/L$ ($D$ is the distance of the moving edge, and $L$ is the length of the substrate) shown in Figure 5c,d. Interestingly, compared to the normal planar tinplate substrates, the laser-cutting tinplate substrates have been given some stress-small "islands", which are separately inlaid in the stress-rich surface of the tinplate substrate. Thus, by designing a reasonable shape/distribution of laser-cutting holes, the mechanical stability can be largely enhanced, as shown in Figure S6. Besides, the simulated von Mises stress distribution of RJ units on the tinplate substrate under convex-up bending and concave-down bending, as well as the stresses extracted at four different places along with the full length of the RJ units, are plotted in Figure 5e−h, which shows that the stresses felt at the top and middle of the RJ units are 2−5 orders of magnitude smaller than those at the root of RJ units and on the surface of tinplate. However, the simulated stresses felt at the surface of the deposited planar thin film are ∼1 order of magnitude larger than those felt on the surface of the tinplate when under convex-up bending, as shown in Figure S8. This indicates that the stresses at the surface of the deposited planar thin film make it easier to approach the failure limit of the a-Si thin film (∼10 GPa),[45,46] which will result in large/long cracks and peeling off segments, especially under convex-up bending. The SiNWs, grown by a Sn-catalyzed VLS process, are welded to the surface of flexible/bendable substrates to protect the out-of-plane RJ portion far away from the stress-rich surface of the flexible/bendable substrates. Thus, the cracks induced by the mechanical bending can only be allowed to spread on the ground surface, without cutting through the standing RJ units, to keep the RJ units continuous and uniform.[29,30]

## 4. CONCLUSIONS

In summary, by incorporating the unique RJ structure directly fabricated upon VLS-grown SiNW framework and semitransparent tinplate substrates prepared by the laser-cutting technology, the semitransparent a-Si:H RJ BIPV devices have been successfully demonstrated in this work. After optimizing the SiNW density, a remarkable $\eta$ of 5.89% has been achieved with a $V_{oc}$ of 0.81 V and a $J_{sc}$ of 12.45 mA/cm$^2$. Such 3D frameworks can not only allow a rather low reflection but also greatly improve the mechanical stability. The laser-cutting substrates can have a designable full-spectral-range transmittance determined by reasonable design and can be compatible with industrial production lines. All these features show a promising potential to develop a new generation of Si-based high-performance, lightweight, low-cost semitransparent thin-film BIPV devices.

## ■ ASSOCIATED CONTENT

### Supporting Information

The Supporting Information is available free of charge at https://pubs.acs.org/doi/10.1021/acsanm.4c03527.

Micrograph, SEM, and EDS elemental mapping images of the tinplate substrate, as well as the schematical diagram of RJ units; SEM images of the tinplate substrates without/with the extra-deposited Sn catalyst, after some fabrication process; SEM images of RJ units with a suitable/higher density; photovoltaic characteristics of the RJ solar cells on AZO glass/tinplate substrates; laser-cutting process and designs for semitransparent tinplate substrates; COMSOL model for simulating the bending-induced stress of normal and laser-cutting tinplate as well as simulated von Mises stress distributions; COMSOL model as well as simulated stress distributions of RJ units on the tinplate

Downloaded from pubs.acs.org/aanmf6/article-pdf/7/17/20536/3190604/an4c03527.pdf by NANJING UNIV user on 04 November 2026



https://doi.org/10.1021/acsanm.4c03527
ACS Appl. Nano Mater. 2024, 7, 20536−20543

substrates; and COMSOL model as well as for simulated stress distributions of the planar thin film deposited on the tinplate substrate (PDF)

## AUTHOR INFORMATION


### Corresponding Authors

**Shaobo Zhang** − *College of Physical Science and Technology/Microelectronics Industry Research Institute, Yangzhou University, 225002 Yangzhou, P. R. China; School of Electronics Science and Engineering/National Laboratory of Solid State Microstructures, Nanjing University, 210023 Nanjing, P. R. China;* orcid.org/0000-0001-7597-3462; Email: shaobozhang@yzu.edu.cn

**Linwei Yu** − *School of Electronics Science and Engineering/National Laboratory of Solid State Microstructures, Nanjing University, 210023 Nanjing, P. R. China;* orcid.org/0000-0002-0801-5210; Email: yulinwei@nju.edu.cn

### Authors

**Shuyi Wang** − *School of Electronics Science and Engineering/National Laboratory of Solid State Microstructures, Nanjing University, 210023 Nanjing, P. R. China*

**Ruijin Hu** − *College of Physical Science and Technology/Microelectronics Industry Research Institute, Yangzhou University, 225002 Yangzhou, P. R. China; School of Electronics Science and Engineering/National Laboratory of Solid State Microstructures, Nanjing University, 210023 Nanjing, P. R. China;* orcid.org/0009-0006-5973-6954

**Yunqing Cao** − *College of Physical Science and Technology/Microelectronics Industry Research Institute, Yangzhou University, 225002 Yangzhou, P. R. China*

**Zongguang Liu** − *College of Physical Science and Technology/Microelectronics Industry Research Institute, Yangzhou University, 225002 Yangzhou, P. R. China;* orcid.org/0000-0003-4141-7462

**Junzhuan Wang** − *School of Electronics Science and Engineering/National Laboratory of Solid State Microstructures, Nanjing University, 210023 Nanjing, P. R. China*

Complete contact information is available at: https://pubs.acs.org/10.1021/acsanm.4c03527


### Notes

The authors declare no competing financial interest.

## ACKNOWLEDGMENTS

The authors acknowledge the financial support from the Special Fund for City School Cooperation of Yangzhou City (no. YZ2022177), Innovation technology platform project jointly built by Yangzhou City and Yangzhou University (no. YZ2020268), Natural Science Foundation of Jiangsu Province (no. BK20230562), National Natural Science Foundation of China (nos. 61974064, 62304200, and 61934004), National Natural Science Foundation of China for Distinguished Young Scholars (no. 62325403), and National Key Research Program of China (grant no. 92164201).

## REFERENCES


(1) Yang, R.; Lee, C.-H.; Cui, B.; Sazonov, A. Flexible Semi-Transparent a-Si:H pin Solar Cells for Functional Energy-Harvesting Applications. *Mater. Sci. Eng., B* **2018**, *229*, 1−5.

(2) Reininghaus, N.; Feser, C.; Hanke, B.; Vehse, M.; Agert, C. Amorphous Single-Junction Cells for Vertical BIPV Application with High Bifaciality. *Energy Sci. Eng.* **2016**, *4* (3), 183−189.

(3) Ng, P. K.; Mithraratne, N.; Kua, H. W. Energy Analysis of Semi-Transparent BIPV in Singapore Buildings. *Energy Build.* **2013**, *66*, 274−281.

(4) Ding, Y.; Young, M.; Zhao, Y.; Traverse, C.; Benard, A.; Lunt, R. R. Influence of Photovoltaic Angle-Dependence on Overall Power Output for Fixed Building Integrated Configurations. *Sol. Energy Mater. Sol. Cells* **2015**, *132*, 523−527.

(5) Martín-Chivelet, N.; Kapsis, K.; Wilson, H. R.; Delisle, V.; Yang, R.; Olivieri, L.; Polo, J.; Eisenlohr, J.; Roy, B.; Maturi, L.; Otnes, G.; Dallapiccola, M.; Upalakshi Wijeratne, W. P. Building-Integrated Photovoltaic (BIPV) Products and Systems: A Review of Energy-Related Behavior. *Energy Build.* **2022**, *262*, 111998.

(6) Peng, C.; Huang, Y.; Wu, Z. Building-Integrated Photovoltaics (BIPV) in Architectural Design in China. *Energy Build.* **2011**, *43* (12), 3592−3598.

(7) An, H.; Yoon, J.; An, Y.; Heo, E. Heating and Cooling Performance of Office Buildings with a-Si BIPV Windows Considering Operating Conditions in Temperate Climates: The Case of Korea. *Sustainability* **2018**, *10* (12), 4856.

(8) Kim, J.; Song, S.; Kim, Y. A Basic Study on Anti-reflection Coating PV Technology for Reducing Reflected Sunlight on the Building Ski. *Asia Pac. J. Converg. Res. Interchange* **2019**, *5* (2), 13−30.

(9) Sung, C. Y. Examining the Effects of Vertical Outdoor Built Environment Characteristics on Indoor Light Pollution. *Build. Environ.* **2022**, *210*, 108724.

(10) Du, J.; Zhang, X.; King, D. An Investigation into the Risk of Night Light Pollution in a Glazed Office Building: The Effect of Shading Solutions. *Build. Environ.* **2018**, *145*, 243−259.

(11) Arnaout, M. A.; Go, Y. I.; Saqaff, A. Pilot Study on Building-Integrated PV: Technical Assessment and Economic Analysis. *Int. J. Energy Res.* **2020**, *44* (12), 9538−9559.

(12) Fazal, M. A.; Rubaiee, S. Progress of PV Cell Technology: Feasibility of Building Materials, Cost, Performance, and Stability. *Sol. Energy* **2023**, *258*, 203−219.

(13) Hughes, L.; Bristow, N.; Korochkina, T.; Sanchez, P.; Gomez, D.; Kettle, J.; Gethin, D. Assessing the Potential of Steel as a Substrate for Building Integrated Photovoltaic Applications. *Appl. Energy* **2018**, *229*, 209−223.

(14) Ahn, K.; Kim, S.-Y.; Kim, S.; Son, D.-H.; Kim, S.-H.; Kim, S.; Kim, J.; Sung, S.-J.; Kim, D.-H.; Kang, J.-K. Flexible High-Efficiency CZTSSe Solar Cells on Stainless Steel Substrates. *J. Mater. Chem. A* **2019**, *7* (43), 24891−24899.

(15) Xu, T.; Luo, Y.; Wu, S.; Deng, B.; Chen, S.; Zhong, Y.; Wang, S.; Leveque, G.; Bachelot, R.; Zhu, F. High-Performance Semi-transparent Organic Solar Cells: From Competing Indexes of Transparency and Efficiency Perspectives. *Adv. Sci.* **2022**, *9* (26), No. e2202150.

(16) Grifoni, F.; Bonomo, M.; Naim, W.; Barbero, N.; Alnasser, T.; Dzeba, I.; Giordano, M.; Tsaturyan, A.; Urbani, M.; Torres, T.; Barolo, C.; Sauvage, F. Toward Sustainable, Colorless, and Transparent Photovoltaics: State of the Art and Perspectives for the Development of Selective Near-Infrared Dye-Sensitized Solar Cells. *Adv. Energy Mater.* **2021**, *11* (43), 2101598.

(17) Zhou, Z.; Yuan, Z.; Yin, Z.; Xue, Q.; Li, N.; Huang, F. Progress of Semitransparent Emerging Photovoltaics for Building Integrated Applications. *Green Energy Environ.* **2024**, *9*, 992.

(18) Yu, H.; Wang, J.; Zhou, Q.; Qin, J.; Wang, Y.; Lu, X.; Cheng, P. Semi-Transparent Organic Photovoltaics. *Chem. Soc. Rev.* **2023**, *52* (13), 4132−4148.

(19) Shen, L.; Yip, H. L.; Gao, F.; Ding, L. Semitransparent Perovskite Solar Cells for Smart Windows. *Sci. Bull.* **2020**, *65* (12), 980−982.

(20) Ritzer, D. B.; Abdollahi Nejand, B.; Ruiz-Preciado, M. A.; Gharibzadeh, S.; Hu, H.; Diercks, A.; Feeney, T.; Richards, B. S.; Abzieher, T.; Paetzold, U. W. Translucent Perovskite Photovoltaics


Downloaded from pubs.acs.org/aanmf6/article-pdf/7/17/20536/3190604/an4c03527.pdf by NANJING UNIV user on 04 November 2026

for Building Integration. *Energy Environ. Sci.* **2023**, *16* (5), 2212−2225.
(21) Yoon, S.; Tak, S.; Kim, J.; Jun, Y.; Kang, K.; Park, J. Application of Transparent Dye-Sensitized Solar Cells to Building Integrated Photovoltaic Systems. *Build. Environ.* **2011**, *46* (10), 1899−1904.
(22) Green, M. A. Third Generation Photovoltaics:Ultra-high Conversion Efficiency at Low Cost. *Prog. Phot. Res. Appl.* **2001**, *9*, 123−135.
(23) Aberle, A. G. Thin-Film Solar Cells. *Thin Solid Films* **2009**, *517*, 4706−4710.
(24) Shah, A. V.; Schade, H.; Vanecek, M.; Meier, J.; Vallat-Sauvain, E.; Wyrsch, N.; Kroll, U.; Droz, C.; Bailat, J. Thin-Film Silicon Solar Cell Technology. *Prog. Phot. Res. Appl.* **2004**, *12* (2−3), 113−142.
(25) Terakawa, A. Review of Thin-Film Silicon Deposition Techniques for High-Efficiency Solar Cells Developed at Panasonic/Sanyo. *Sol. Energy Mater. Sol. Cells* **2013**, *119*, 204−208.
(26) You, D. J.; Kim, S. H.; Lee, H.; Chung, J.-W.; Hwang, S.-T.; Heo, Y. H.; Lee, S.; Lee, H.-M. Recent Progress of High Efficiency Si Thin-Film Solar Cells in Large Area. *Prog. Phot. Res. Appl.* **2015**, *23* (8), 973−988.
(27) D'yakonov, A. A.; Moleva, O. N.; Mel'nikov, Y. A.; Nikiforov, M. A.; Vakil'ev, A. F. Improving Tinplate Production. *Steel Transl.* **2012**, *42* (3), 253−254.
(28) Keles, O.; Dundar, M. Aluminum Foil: Its Typical Quality Problems and Their Causes. *J. Mater. Process. Technol.* **2007**, *186*, 125−137.
(29) Zhang, S.; Zhang, T.; Liu, Z.; Wang, J.; Xu, J.; Chen, K.; Yu, L. Flexible and Robust 3D a-SiGe Radial Junction Near-Infrared Photodetectors for Rapid Sphygmic Signal Monitoring. *Adv. Funct. Mater.* **2022**, *32*, 2107040.
(30) Sun, X.; Zhang, T.; Wang, J.; Yang, F.; Xu, L.; Xu, J.; Shi, Y.; Chen, K.; Roca i Cabarrocas, P.; Yu, L. Firmly Standing Three-Dimensional Radial Junctions on Soft Aluminum Foils Enable Extremely Low Cost Flexible Thin Film Solar Cells with Very High Power-to-Weight Performance. *Nano Energy* **2018**, *53*, 83−90.
(31) Yu, L.; Misra, S.; Wang, J.; Qian, S.; Foldyna, M.; Xu, J.; Shi, Y.; Johnson, E.; Cabarrocas, P. R. i. Understanding Light Harvesting in Radial Junction Amorphous Silicon Thin Film Solar Cells. *Sci. Rep.* **2014**, *4*, 4357.
(32) Zhang, S.; Zhang, T.; Liu, Z.; Wang, J.; Yu, L.; Xu, J.; Chen, K.; Roca i Cabarrocas, P. Highly Flexible Radial Tandem Junction Thin Film Solar Cells with Excellent Power-to-Weight Ratio. *Nano Energy* **2021**, *86*, 106121.
(33) Misra, S.; Yu, L.; Chen, W.; Foldyna, M.; Cabarrocas, P. R. i. A review on plasma-assisted VLS synthesis of silicon nanowires and radial junction solar cells. *J. Phys. D: Appl. Phys.* **2014**, *47* (39), 393001.
(34) Yu, L.; O'Donnell, B.; Alet, P. J.; Conesa-Boj, S.; Peiro, F.; Arbiol, J.; Cabarrocas, P. R. Plasma-Enhanced Low Temperature Growth of Silicon Nanowires and Hierarchical Structures by Using Tin and Indium Catalysts. *Nanotechnology* **2009**, *20* (22), 225604.
(35) Zardo, I.; Yu, L.; Conesa-Boj, S.; Estrade, S.; Alet, P. J.; Rossler, J.; Frimmer, M.; Roca i Cabarrocas, P.; Peiro, F.; Arbiol, J.; Morante, J. R.; Fontcuberta i Morral, A. Gallium Assisted Plasma Enhanced Chemical Vapor Deposition of Silicon Nanowires. *Nanotechnology* **2009**, *20* (15), 155602.
(36) Yu, L.; Fortuna, F.; O'Donnell, B.; Jeon, T.; Foldyna, M.; Picardi, G.; Roca i Cabarrocas, P. Bismuth-Catalyzed and Doped Silicon Nanowires for One-Pump-Down Fabrication of Radial Junction Solar Cells. *Nano Lett.* **2012**, *12*, 4153−4158.
(37) Zhang, S.; Huang, H.; Zhang, Z.; Feng, J.; Liu, Z.; Wang, J.; Xu, J.; Li, Z.; Yu, L.; Chen, K.; Zou, Z. Ultrathin 3D radial tandem-junction photocathode with a high onset potential of 1.15 V for solar hydrogen production. *Chin. J. Catal.* **2022**, *43* (7), 1842−1850.
(38) Xie, X.; Zeng, X.; Yang, P.; Li, H.; Li, J.; Zhang, X.; Wang, Q. Radial n-i-p Structure SiNW-Based Microcrystalline Silicon Thin-Film Solar Cells on Flexible Stainless Steel. *Nanoscale Res. Lett.* **2012**, *7*, 621.
(39) Xie, X.; Zeng, X.; Yang, P.; Li, H.; Li, J.; Zhang, X.; Wang, Q. Radial n-i-p Structure Silicon Nanowire-Based Solar Cells on Flexible Stainless Steel Substrates. *Phys. Status Solidi A* **2013**, *210* (2), 341−344.
(40) Madaka, R.; Kanneboina, V.; Agarwal, P. Exploring the Photo Paper as Flexible Substrate for Fabrication of a-Si:H Based Thin Film Solar Cells at Low Temperature (110 °C): Influence of Radio Frequency Power on Opto-Electronic Properties. *Thin Solid Films* **2018**, *662*, 155−164.
(41) Cho, J.-S.; Baek, S.; Lee, J. C. Surface Texturing of Sputtered ZnO:Al/Ag Back Reflectors for Flexible Silicon Thin-Film Solar Cells. *Sol. Energy Mater. Sol. Cells* **2011**, *95* (7), 1852−1858.
(42) Dong, W. J.; Yoo, C. J.; Cho, H. W.; Kim, K. B.; Kim, M.; Lee, J. L. Flexible a-Si:H Solar Cells with Spontaneously Formed Parabolic Nanostructures on a Hexagonal-Pyramid Reflector. *Small* **2015**, *11* (16), 1947−1953.
(43) Lin, Q.; Lu, L.; Tavakoli, M. M.; Zhang, C.; Lui, G. C.; Chen, Z.; Chen, X.; Tang, L.; Zhang, D.; Lin, Y.; Chang, P.; Li, D.; Fan, Z. High Performance Thin Film Solar Cells on Plastic Substrates with Nanostructure-Enhanced Flexibility. *Nano Energy* **2016**, *22*, 539−547.
(44) Das, G.; Mandal, S.; Dhar, S.; Bhargav, P. B.; Banerjee, C.; Mukhopadhyay, S.; Barua, A. K. Synthesis of ITO nanoparticles at room temperature using plasma treatment process and use it as back reflector in a-Si flexible solar cell. *Surf. Interfaces* **2017**, *7*, 83−86.
(45) Follstaedt, D. M.; Knapp, J. A.; Myers, S. M. Mechanical properties of ion-implanted amorphous silicon. *J. Mater. Res.* **2004**, *19* (1), 338−346.
(46) Hengst, C.; Menzel, S. B.; Rane, G. K.; Smirnov, V.; Wilken, K.; Leszczynska, B.; Fischer, D.; Prager, N. Mechanical Properties of ZTO, ITO, and a-Si:H Multilayer Films for Flexible Thin Film Solar Cells. *Materials* **2017**, *10* (3), 245.

Downloaded from pubs.acs.org/aanmf6/article-pdf/7/17/20536/3190604/an4c03527.pdf by NANJING UNIV user on 04 November 2026


https://doi.org/10.1021/acsanm.4c03527
*ACS Appl. Nano Mater.* 2024, 7, 20536−20543